Chemical Physics 80 (1983) 157–165
North-Holland Publishing Company

VIBRATIONAL EFFECTS WITH EXCITATION TRANSFER IN METASTABLE RARE-GAS–HALIDE COLLISIONS

Mattanjah S. DE VRIES and Richard M. MARTIN

Department of Chemistry, University of California, Santa Barbara, California 93106, USA

Received 16 February 1983; in final form 13 May 1983

Collisions of $Ar(^3P_{2,0})$ and $Kr(^3P_{2,0})$ with Cl_2 and Br_2 were studied over the collision energy range 0.01–0.5 eV, using a crossed-beam time-of-flight technique. The dependence of the total chemiluminescence cross sections (from excimer formation plus excitation transfer) on collision energy follows the behavior expected from the orbiting-controlled curve-crossing model. The energy dependence for excitation transfer does not follow this model, and is quite different for Cl_2 versus Br_2. These results are explained by a phase-matching curve-crossing model, in terms of the A^+/X_2^- trajectory motion and the phase of the X_2^- vibrational motion.

1. Introduction

There exist close similarities between metastable rare-gas atoms (A*) and alkali-metal atoms (M) [1–3]. Collisions of both types of atoms with halogen molecules (X_2) are characterized by crossings from neutral to ionic potential curves at large internuclear distances, leading to halide-atom transfer (AT) reactions,

$$A^* + X_2 \rightarrow AX^* + X, \qquad \text{AT}$$
$$M + X_2 \rightarrow MX + X. \qquad (1)$$

These thermal reactions proceed via an intermediate ion-pair state, but ion-pair formation (IPF) as final products is only possible at energies above $E = IP - EA$, where E is the relative translational (and internal) energy of the collision partners. IP is the ionization potential of the metastable or alkali atom, and EA is the electron affinity of the halogen.

$$A^* + X_2 \rightarrow A^+ + X_2^-, \qquad \text{IPF}$$
$$M + X_2 \rightarrow M^+ + X_2^-. \qquad (2)$$

The metastables are sometimes described as alkali atoms with a core hole, or "superalkalis". As a result of the large amount of electronic excitation energy carried by the metastables, several competing processes may occur that are absent with the alkalis, e.g., excitation transfer (ET) and Penning ionization (PI):

$$A^* + X_2 \rightarrow A + X_2^*, \qquad \text{ET} \qquad (3)$$
$$A^* + X_2 \rightarrow A + X_2^+ + e, \qquad \text{PI} \qquad (4)$$

At thermal energies alkali systems only have channel (1) available, while metastable systems can have channels (1), (3) and (4) available. Alkali/halogen collisions have been extensively studied and are well understood [4]. It is therefore of interest to study the counterpart metastable collisions, with emphasis on the additional competative channels.

Most of the available information on thermal $A^* + X_2$ reaction channels derives from flowing-afterglow experiments [5]. They show that the general features are the same as with thermal $M + X_2$ reactions, but there are also significant differences, in particular in the energy disposal. Some molecular-beam experiments have also been done with these systems. Gillen et al. [2,3] have studied differential cross sections for ion-pair formation in fast collisions of Ar* with I_2, and compared the results with the analogous reactions of $K + I_2$.

0301-0104/83/0000–0000/$03.00 © North-Holland

Their results show that the behavior of the two systems is nearly the same, showing that the IPF process is not much influenced by the core hole in the rare-gas atom. Simons and co-workers [6,7] have used a hyperthermal rotor-accelerated atom-beam to study the collisional energy dependence of the Kr*, Xe^*/Br_2 excimer formation cross sections, and have also studied the energy dependence of the chemiluminescence polarization.

In the present work we have studied the collisional energy depenence of reaction (3) with the Ar*, Kr^*/Cl_2, Br_2 systems in the thermal energy region. Reaction (3) competes with the major reaction (1), which yields excimers. Both reactions take place via the ion-pair intermediate shown in reaction (2). Reaction (3) involves a second crossing from the intermediate ionic curve back to a neutral curve correlating with X_2^*. This second crossing depends strongly on the vibrational amplitude of the X_2^- intermediate ion, and therefore the relationship between the vibrational period and the collision time becomes important in determining the energy-transfer cross section. This vibrational phase-matching effect has been seen previously in studies of ion-pair formation in fast M/X_2 collisions [8]. In this work we demonstrate the importance of vibrational-phase matching in controlling energy transfer in thermal A^*/X_2 collisions.

2. Experimental

The experimental method has been described in detail elsewhere [9]. Fig. 1 shows the experimental arrangement used in this work. An effusive beam from the rare-gas source passed through a Penning (cold cathode) gas discharge, a pulser wheel and sweeper plates. Ions and high Rydberg states are not expected to escape the high electric and magnetic fields of the Penning source. However, the sweeper plates with a dc field of 1 kV/cm were provided as a precaution to eliminate any stray ions or high Rydberg states in the beam. The pulsed beam containing only ground-state and

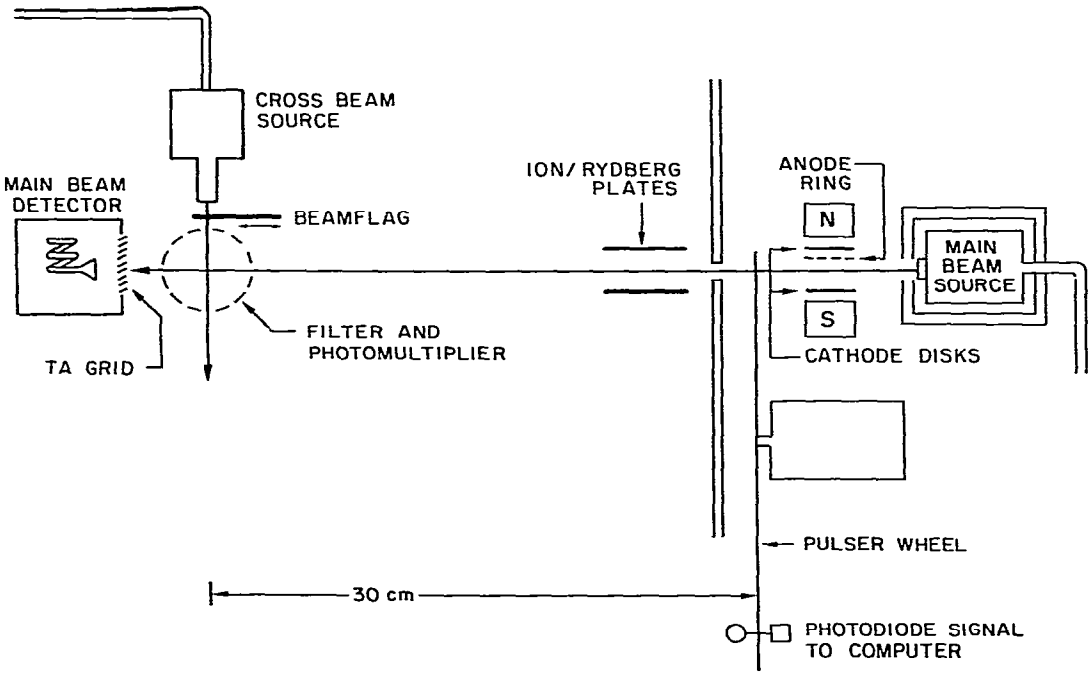

Fig. 1. Schematic diagram of the apparatus.

metastable rare-gas atoms impinged on a tantalum ribbon detector and the ejected electrons were detected by a channel electron multiplier. The A* beam traversed the effusive X_2 beam emerging from the halogen source, and the chemiluminescence from the interaction region passed through a light filter and was detected by a EMI 9750 photomultiplier tube. Both photons and metastables were counted as a function of arrival time, using a home-built multichannel scaler interface to a minicomputer. The halide beam was modulated by a chopper to provide for background measurement and subtraction. Various light filters were used to isolate the chemiluminescence from different products. A Corning 7-54 lightfilter was used to isolate the KrCl* and KrBr* chemiluminescence in the 200–300 nm region. The ArX* emission and X* emission from ArX* predissociation are in the 100–200 nm region, and were observed using a Corning 5-54 filter coated with 1 mg/cm^2 of sodium salicilate [10]. The VUV emission absorbed by the sodium salicilate gives broad fluorescence emission in the near UV region, most of which passes the 5-54 filter to be detected by the photomultiplier tube. Interference filters with 10 nm bandwidths were used for isolating the X_2^* emission. The filters were centered on 250 nm for Cl_2^* and 290 nm for Br_2^*, corresponding to the maxima in the respective emission bands.

3. Results and discussion

3.1. Total cross sections

We have obtained the collisional energy dependence of the total chemiluninescence cross sections for the four systems of Ar($^3P_{0,2}$) and Kr($^3P_{0,2}$) with Cl_2 and Br_2. The sodium salicilate coated filter, which was used to detect the Ar excimers, has a flat wavelength response over the entire spectral region of interest. This means that the detection efficiency is constant, even if the emission spectrum changes with velocity. With the Corning 7-54 filter used in the detection of the Kr excimers, the detection efficiency might become velocity dependent if the emission spectrum were

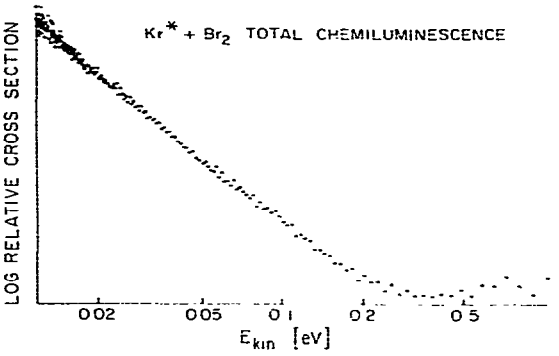

Fig. 2. Logarithmic plot of total chemiluminescence versus relative energy for the reaction of Kr* with Br_2.

to change with velocity. However, such effects are likely to be very small.

In all cases the total chemiluminescence cross section σ_T is found to be proportional to E^{-m}, where E is the relative kinetic energy and m is a constant. Therefore $\ln(\sigma_T) \propto -m \ln(E)$, as shown in fig. 2 for the Kr*/Br_2 system. The E^{-m} cross-section dependence holds up to an energy E_{max} of 0.1–0.2 eV, after which the cross section levels off. This behavior is readily explained by the orbiting-controlled curve-crossing model [11]. In this model, collision processes are governed at low energies by a long-range attractive potential of the form C/R^s. The orbiting cross section for a kinetic energy E is given by

$$\sigma_0 = \pi b_0^2 = \pi \left(\frac{s}{s-2}\right)\left(\frac{s-2}{2}\frac{C}{E}\right)^{2/s}. \tag{5}$$

Here b_0 is the maximum impact parameter for which the centrifugal barrier can be surmounted. The position of that barrier is given by:

$$R_0 = \tfrac{1}{2}(s-2)(C/E)^{1/s}. \tag{6}$$

The ion-pair curve crosses the neutral curve at a distance R_c, given approximately by

$$e^2/R_c = \mathrm{IP} - \mathrm{EA}. \tag{7}$$

The neutral and ionic curves are shown schematically in fig. 3. When the internuclear distance R_c is reached an electron jump takes place and the system proceeds on the ionic potential, leading to

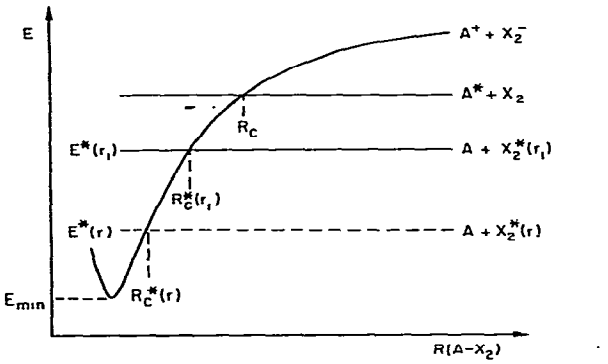

Fig. 3. Schematic potential energy diagram. As X_2^- vibrates following electron transfer at R_c, the $A+X_2^*$ energy level oscillates with respect to the $A^+ + X_2^-$ level. $E^*(r_1)$ is the maximum X_2^* energy level (see fig. 4), which crosses the ionic curve at $R_c^*(r_1)$. As the X_2^- internuclear distance increases due to the X_2^- vibrational expansion, $E^*(r)$ decreases (as shown in fig. 4) giving a smaller crossing distance $R_c^*(r)$. The minimum value of $E^*(r)$ may be above or below the ionic-potential minimum E_{min}.

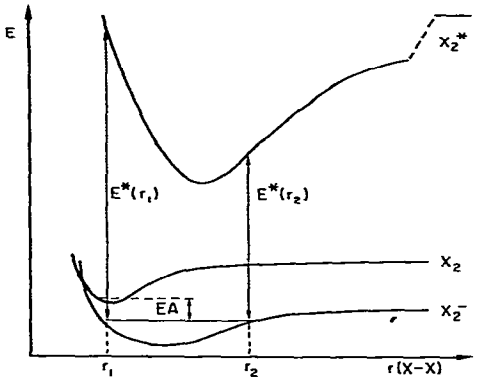

Fig. 4. Schematic potential-energy diagram as a function of halogen internuclear distance, at a fixed $A-X_2$ distance. EA is the vertical electron affinity of X_2 at r_1. After the transition, X_2^- vibrates between r_1 and r_2.

reaction with near unit probability. Therefore the total reaction-cross-section energy dependence can be described by eq. (5) for $R_0 > R_c$. Setting $R_c = R_0$ in eq. (6), the maximum energy for which $\sigma_T \propto E^{-m}$ should hold is approximately

$$E_{max} = [(s-2)/2]^s C/R_c^s. \quad (8)$$

For larger energies the cross section is expected to level off, since on the ionic $1/R$ potential there is no centrifugal barrier.

Table 1 shows the values for s and E_{max}, obtained from plots such as fig. 2. The fact that s in most cases is lower than 6 seems to indicate long-range adiabatic potentials that are more attractive than unperturbed r^{-6} (van der Waals) potentials. The values of C were calculated using the Slater–Kirkwood approximation [12], and eq. (8) was then used to estimate R_c. The results for R_c are all of the order of 5 Å, as expected from the harpoon model. According to that model the crossing distance can be calculated with eq. (7). Using an "effective" EA of 1.9 eV for X_2, in accordance with the results of the alkali/halogen studies [14], we obtain R_c values of 6.2 Å for the Ar systems

Table 1
Dynamical parameters for $A^* + X_2$ total chemiluminescence reactions

Reactant	s [a] (±0.4)	E_{max} [b] (±0.05 eV)	C [c] (eV Å^6)	R_c [d] (Å)	EA_{eff} [e] (eV)	EA [f] (eV)
$Ar^* + Cl_2$	5.2	0.13	431	5.2	1.4	2.4
$Ar^* + Br_2$	6.2	0.12	590	4.4	0.8	2.5
$Kr^* + Cl_2$	4.7	0.11	445	6.2	1.8	2.4
$Kr^* + Br_2$	5.5	0.20	609	4.8	1.1	2.5

[a] The long-range potential is $V = C/R^s$, and $s = 2/m$, where m is determined from the experimental-cross-section energy dependence, $\sigma \propto E^{-m}$.
[b] The maximum energy for which $\sigma \propto E^{-m}$.
[c] See ref. [12]. [d] Determined from eq. (8).
[e] The effective halogen-molecule electron affinities from eq. (7). Since EA_{eff} is a dynamical variable, it may depend on A^* as well as on X_2 (see text).
[f] Thermochemical halogen-molecule electron affinities from ref. [13].

and 6.6 Å for the Kr systems. Alternatively the effective (or "reactive") electron affinity can be calculated using eq. (7) and the R_c values estimated from eq. (8). Those results are also given in table 1, together with the thermochemical electron affinities. The effective EAs are less than the thermochemical EAs, as illustrated by the schematic X_2 and X_2^- potential energy diagram shown in fig. 4. The thermochemical EA corresponds approximately to the difference in the X_2^- and X_2 ground-state levels. The effective EA should correspond roughly to the vertical EA shown. However, the EA_{eff} is in fact a dynamical variable, since it is the vertical EA of the X_2 molecule *perturbed by the approaching A* atom.* Therefore the EA_{eff} values may depend on A* as well as X_2, as found in table 1.

3.2. Excitation transfer

According to flowing-afterglow experiments with these systems, AT is the dominant reaction and ET is a relatively small reaction channel [5]. The available information is summarized in table 2, and will be discussed below. Penning ionization

Table 2
Percentage of quenching cross sections due to excitation transfer for $A^* + X_2$ systems. See ref. [5]

Reagent	Cl_2	Br_2	I_2
Ar*	3	7	
Kr*	12	25	
Xe*	0	2	20

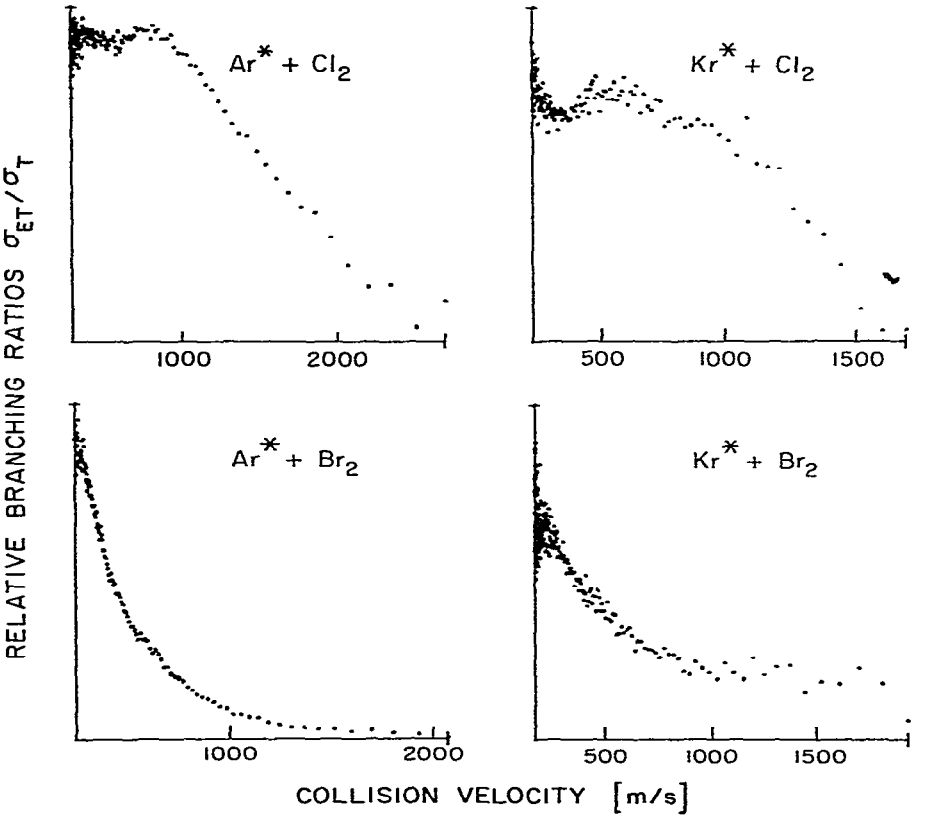

Fig. 5. Relative branching ratios for excitation of Cl_2 and Br_2 as a function of collision velocity. Halogen emission is divided by total chemiluminescence to give the relative cross section σ_{ET}/σ_T.

is unimportant for these systems: with Kr it is energetically inaccesible, while with Ar it constitutes less than 1% of the total cross section [5,15]. For ET and AT alike the collisional energy dependence of the reaction cross section below E_{max} is mainly determined by the long-range forces, i.e., the "close collision" or "orbiting" cross section described above. Any effect on the cross section for a specific reaction channel which is due to the collision dynamics at shorter internuclear distances must be superimposed onto that strong behavior and is therefore difficult to observe. In order to bring out the dynamics of ET we have divided the halogen fluorescence signal by the total chemiluninescence signal, to give the relative branching ratio $\sigma_{E:T}/\sigma_T$ as a function of collision energy. The results are shown in fig. 5. The results with Kr are seen to be noisier because in those cases the excited-halogen radiation overlaps that of the excimer. As a result the ET channel could not be separated as well as in the Ar cases.

It is clear that systems with different rare gases behave alike, while systems with different halogen molecules do not. We propose the following model. Referring to fig. 3, it is known that at thermal energies nearly all trajectories that reach the crossing distance R_c will proceed on the ionic surface [4]. Trajectories that entirely follow the ionic surface may be assumed to lead to atom transfer. For ET to occur, a second crossing must take place from the ionic surface onto a $A + X_2^*$ potential which crosses the ionic surface at R_c^* (fig. 3). In considering the possible second crossing we note that one-electron processes are much more probable than two-electron rearrangements. The $^3\Pi_{2g}$ state can be formed from X_2^- by a one-electron transition, since its electron configuration is $\sigma^2\pi^3\pi^4\sigma$ while that of the negative ion is $\sigma^2\pi^4\pi^4\sigma$. The only other possibility is the $1\,^3\Sigma_u^+$ state with a $\sigma\pi^4\pi^4\sigma$ configuration. Other states with a suitable electron configuration are unbound and lie below the ionic potential well [16,17]. We therefore assign the halogen fluorescence to the $^3\Pi_{2g}$ state. Although there are a large number of other excited halogen states that are energetically accessible, there are several arguments to support this assignment. First of all it is consistant with the wavelength of the emission isolated by our interference filters [5,18]. It is also close to the radiation involved with halogen UV laser action, which is assigned to this level [19]. Population of such a state through a cascade from higher Rydberg states is unlikely, because of the long lifetimes expected for such states [20]. Molecules in high Rydberg states would escape the observation region of our experiments before being detected. Gundel et al. [18] note that in their experiments with $Ar^* + Cl_2$ they did not observe high Rydberg states of Cl_2. We have performed a check by applying an electrostatic field in the interaction region, that would quench any high Rydberg states if they were formed. Even with a field of 2 kV/cm there was no decrease in chemiluminescence intensity, and no ions (which would be formed by high Rydberg quenching) were observed.

Finally we note that the reverse reaction has also been observed [21]: $A + X_2^* \rightarrow AX^* + X$. This process has a large cross section when the halogen is excited to a specific energy level, of the order of 10 eV. This is consistent with the assumption, made above, that a specific X_2^* couples efficiently (i.e., via a one-electron transfer) with the ionic potential, providing an ionic intermediate mechanism for the reverse reaction.

3.3. *Phase-matching model for excitation transfer*

The assumption made at this point is that the probability for the trajectories on the ion-pair potential to pass through a second crossing to the $A + X_2^*$ potential depends upon the internuclear distance r of the X_2^-. The effects of bond stretching on the crossing probability are well known from M/X_2 studies [4]. As shown in fig. 4, X_2^- has a larger equilibrium distance than X_2, causing it to be formed in an excited vibrational state. The bond-length varies between r_1 and r_2, and (as can be seen in fig. 4) the energy $E^*(r)$ of X_2^* depends strongly upon r. As the X_2^- bond stretches $E^*(r)$ decreases, and therefore the second crossing distance decreases, i.e., the E^* level in fig. 3 moves down, causing it to cross the ionic curve at a smaller R_c^*. The result is that the incoming trajectory sees the second crossing distance R_c^* vibrating as a breathing sphere, due to the vibrational motion of X_2^-. The total probability for the $A^+ + X_2^-$

trajectories to reach $R_c^*(r)$ and to cross to the $A + X_2^*$ curve is affected by the X_2^- vibration in a number of ways:

(i) The coupling-matrix element depends exponentially upon the $V_i - V^*$ crossing distance [20], where V_i is the ion-pair potential and V^* is the $A + X_2^*$ potential. This means that for smaller values of R_c^* (occurring when r is large) the potentials are more adiabatic and an electron jump is more likely.

(ii) The total coupling-matrix element also depends upon the X_2^- to X_2^* vibrational-transition matrix element, which is more favorable when the molecular ion is stretched.

(iii) Obviously, if $E^*(r)$ drops below E_{min} (the bottom of the ionic potential well) the ET channel is cut off completely.

(iv) In the Landau–Zener model the crossing probability also depends on the relative velocity. In this case that is the relative velocity of $A^+ + X_2^-$ with respect to the motion of the crossing distance R_c^* [22].

For all these reasons the phase of the X_2^- vibration at the time the second crossing R_c^* is reached determines the crossing probability. The important collision trajectory parameter is the time t_c required for the trajectory to pass from R_c to R_c^*, as compared to the vibrational period τ of the X_2^-. In order to illustrate the phase-matching conditions between τ and t_c which allow excitation transfer to occur, we have performed simple trajectory calculations, assuming zero impact-parameter collisions. The Coulomb potential was used for $A^+ + X_2^-$, and a harmonic oscillator potential was used for X_2^-, corresponding to the X_2^- ground-vibrational-state frequency [17]. $R(A^+–X_2^-)$ and $R_c^*(r)$ were calculated as a function of time following the crossing to the ionic potential at R_c on the incoming trajectory. The results for $Ar^* + Cl_2$ collisions are shown in fig. 6. At $t = 0$ the system is at R_c with its initial relative velocity and the particles begin their acceleration along the Coulomb potential (fig. 3). $R(Ar^+–Cl_2^-)$ is shown as a function of time for different initial collision velocities. At $t = 0$ the Cl_2^- vibration also begins its expansion phase (fig. 4), causing E^* to drop below E_{min}, as shown by the dashed line in fig. 6. ET cannot occur for the high-velocity trajectories, because they arrive at E_{min} before the Cl_2^- contraction phase returns E^* above E_{min}. There is a range of low velocities which arrive at R_c^* during the contraction phase when $E^* > E_{min}$, and this temporal region determines the velocity range where ET can occur. Furthermore, there should be a velocity in this range which gives a minimum in the ET cross section, corresponding to one complete Cl_2^- vibration, because the coupling matrix element is smallest when r is smallest. These qualitative observations are in agreement with the results shown in fig. 5 for $Ar^* + Cl_2$.

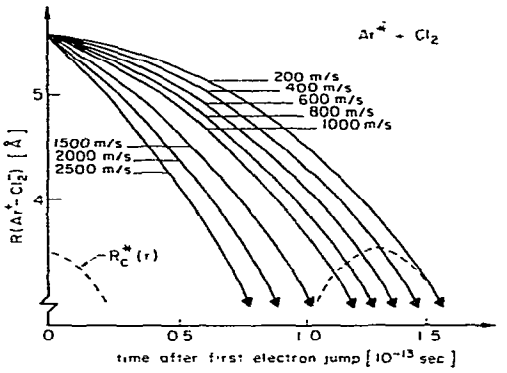

Fig. 6. Calculated $Ar^+–Cl_2^-$ distance as a function of time following the first crossing at R_c, for different initial $Ar^+–Cl_2^-$ relative velocities. The broken line indicates the location of the second crossing point R_c^* as a function of time determined by the Cl_2^- vibration. R_c^* exists only when $E^* > E_{min}$ (see figs. 3 and 4).

The above discussion and the calculated results shown in fig. 6 are for zero impact-parameter collisions of Ar* with Cl_2. In the thermal collision-energy region, A^*/X_2 reactions are dominated by large impact-parameter reactive trajectories. The radial velocities of these trajectories are slower than those of small impact-parameter trajectories with the same initial relative velocity. The presence of all impact parameters will smear out the results predicted by plots such as fig. 6, but the qualitative conclusions remain the same. The present simple model also ignores complications which may occur after crossing to the $A + X_2^*$ potential, such as possible coupling with other potentials at short range, and recrossing to the ionic potential on the outgoing trajectory.

It can now be understood why the excitation-transfer velocity dependence is so different for different molecules. Replacing Cl_2 by Br_2 has two effects: the vibration is slower and the energy of the excited molecule is lower. As a result, only the very slow trajectories will reach the second crossing after a Br_2^- vibrational period, when E^* is above E_{min}. The main effect of replacing Ar by Kr is to shift the energy levels. The energy of $Kr(^3P_2)$ is lower than that of $Ar(^3P_2)$ by 1.6 eV. This lowers the Kr^+–Cl_2^- curve, and as a result $E^*(r)$ remains above E_{min} throughout the Cl_2^- vibration. The resultant trajectories are sketched in fig. 7 for Kr^*/Cl_2. For specific initial velocities R^* may now be passed several times during the trajectory. The cross-section energy dependence is therefore more complex, and more sophisticated calculations are required to predict the form of σ_{ET}/σ_T.

The calculations described above are based on approximate models and parameters. For example, the diatomic-potential curves of fig. 4 are perturbed by the presence of A*, and are therefore a function of $R(A–X_2)$, which is a function of the $A–X_2$ trajectory [23]. There are also important parameters that are not accurately known, such as the vertical electron affinities of the halogen molecules and the values of $E^*(r)$. We estimate the excitation energy for the $^3\Pi_{2g}$ state of the halogens to be of the order of 10 eV for Cl_2 and Br_2 and of the order of 8 eV for I_2. This may be helpful for understanding the different branching ratios, considering that the $^3P_2$ levels for Ar, Kr and Xe are at 11.5, 9.9 and 8.3 eV, respectively [24]. Excitation transfer seems to compete with atom transfer most effectively in those cases where the excitation energy of the halogen is close to the metastable level and therefore $R_c^*(r_1)$ is close to R_c. This is because the phase matching for such systems is like that of fig. 7 rather than fig. 6. The curve-crossing probability is expected to be further enhanced for large impact-parameter collisions, which – slowed down by the centrifugal potential – spend more time on the intermediate ionic surface. Hennessy and Simons [7] observed in polarization measurements that KrBr* formed in $Kr^* + Br_2$ reactions is significantly less rotationally alligned than XeBr* formed in $Xe^* + Br_2$ reactions. Kr^*/Br_2 also has the largest branching ratio for ET (table 2). The trajectories leading to ET instead of AT are apparently those that would otherwise have caused a large product alignment, i.e. the ones with large impact parameters, consistent with our model.

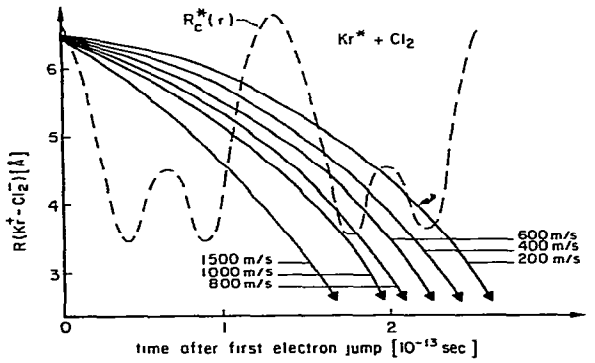

Fig. 7. Same as fig. 6, for Kr^+–Cl_2^-. With this system $E^*(r_m) > E_{min}$ throughout the Cl_2^- vibrational motion. R_c^* has its maximum when the Cl_2^- vibration is at its inner turning point. A second (smaller) maximum results when the Cl_2^- vibration reaches its outer turning point.

Simons [25] has proposed a different model to explain the ET/AT branching ratios, assuming more attractive $A^* + X_2$ potentials that would cross with the $A + X_2^*$ surface, rather than with the ionic surface. This underscores the fact that more accurate potentials are required in order to fully understand these systems. However, we conclude that our exprimental results are well described by a model based on crossing from the $A^* + X_2$ surface to the $A^+ + X_2^-$ surface, followed by crossing to the $A + X_2^*$ surface with a probability which is a function of phase matching between the collision trajectory and the vibrational motion of X_2^-.

Acknowledgement

The authors would like to thank J. Los, A.W. Kleyn and E. Gislason for stimulating discussions. We are also grateful to the US Department of Energy Office of Basic Energy Sciences for the support of this research (Grant DE-AM03-765F00034).

References

[1] D.W. Setser, T.D. Dreiling, H.C. Brashears and J.H. Kolts, Faraday Discussions Chem. Soc. 67 (1978) 1613.
[2] K.T. Gillen, T.D. Gaily and D.C. Lorents, Chem. Phys. Letters 57 (1978) 192.
[3] A.P. Hickman and K.T. Gillen, J. Chem. Phys. 73 (1980) 3672.
[4] J. Los and A.W. Kleyn, in: Alkali halide vapors, eds. P. Davidovits and D.L. McFadden (Academic Press, New York, 1979).
[5] K. Tamagake, D.W. Setser and J.H. Kolts, J. Chem. Phys. 74 (1981) 4286.
[6] C.T. Rettner and J.P. Simons, Chem. Phys. Letters 59 (1978) 178.
[7] R.J. Hennessy and J.P. Simons, Chem. Phys. Letters 75 (1980) 43.
[8] A.W. Kleyn, J. Los and E.A. Gislason, Phys. Rep. 90 (1982) 1.
[9] T.P. Parr and R.M. Martin, J. Chem. Phys. 69 (1978) 1613.
[10] J.A.R. Samson, Techniques of VUV spectroscopy (Wiley, New York, 1967) p. 212.
[11] R. Grice and D.R. Herschbach, Mol. Phys. 27 (1974) 159.
[12] E.A. Gislason, private communication;
E.W. McDaniel and E.A. Mason, The mobility and diffusion of ions in gases, (Wiley–Interscience, New York, 1973) p. 346.
[13] P.S. Drzaic, J. Marks and J.I. Brauman, Gas-phase ion chemistry, Vol. 3, ed. M.T. Bowers (Academic Press, New York) to be published.
[14] E.A. Gislason, in: Alkali halide vapors, eds. P. Davidovits and D.L. McFadden (Academic Press, New York, 1979).
[15] D.M. Hanson-Parr, Ph.D. Thesis, University of California, Santa Barbara (1980).
[16] R.S. Mulliken, J. Chem. Phys. 55 (1971) 288.
[17] S.D. Peyerimhoff and R.J. Buenker, Chem. Phys. 57 (1981) 279.
[18] L.A. Gundel, D.W. Setser, M.A.A. Clyne, J.A. Coxon and W. Nip, J. Chem. Phys. 64 (1976) 4390.
[19] M. Diegelmann, K. Hohla, F. Rebentrost and K.L. Kompa, J. Chem. Phys. 76 (1982) 1233.
[20] R.D. Rundel, private communication.
[21] M.C. Castex, J. Le Calve, D. Haaks, B. Jordan and G. Zimmer, Chem. Phys. Letters 70 (1980) 106.
[22] R.E. Olson, F.T. Smith and E. Bauer, Appl. Opt. 10 (1971) 1848.
[23] E.A. Gislason, A.W. Kleyn and J. Los, Chem. Phys. 59 (1981) 91.
[24] C.E. Moore, ed., Atomic energy levels, Vols. 1–3, National Bureau of Standards Circular 467 (US Govert. Printing Office, Washington, 1958).
[25] J.P. Simons, Chem. Phys. Letters 91 (1982) 484.